Applied Surface Science 389 (2016) 967–976

Contents lists available at ScienceDirect

Applied Surface Science

journal homepage: www.elsevier.com/locate/apsusc

Surface modification of tube inner wall by transferred atmospheric pressure plasma

Faze Chen[a], Shuo Liu[a], Jiyu Liu[a], Shuai Huang[a], Guangqing Xia[b], Jinlong Song[a], Wenji Xu[a], Jing Sun[a], Xin Liu[a,*]

[a] Key Laboratory for Precision and Non-Traditional Machining Technology of Ministry of Education, Dalian University of Technology, Dalian 116024, China
[b] State Key Laboratory of Structure Analysis for Industrial Equipment, Dalian University of Technology, Dalian 116024, China

ARTICLE INFO

Article history:
Received 21 March 2016
Received in revised form 13 July 2016
Accepted 7 August 2016
Available online 9 August 2016

Keywords:
Atmospheric pressure plasma
Tube
Wettability
Surface modification
Aging

ABSTRACT

Tubes are indispensable in our daily life, mechanical engineering and biomedical fields. However, the practical applications of tubes are sometimes limited by their poor wettability. Reported herein is hydrophilization of the tube inner wall by transferred atmospheric pressure plasma (TAPP). An Ar atmospheric pressure plasma jet (APPJ) is used to induce He TAPP inside polytetrafluoroethylene (PTFE) tube to perform inner wall surface modification. Optical emission spectrum (OES) is used to investigate the distribution of active species, which are known as enablers for surface modification, along the TAPP. Tubes' surface properties demonstrate that after TAPP treatment, the wettability of the tube inner wall is well improved due to the decrease of surface roughness, the removal of surface fluorine and introduction of oxygen. Notably, a deep surface modification can significantly retard the aging of the obtained hydrophilicity. The results presented here clearly demonstrate the great potential of TAPP for surface modification of the inner wall of tube or other hollow bodies, and thus a uniform, effective and long-lasting surface modification of tube with any length can be easily realized by moving the tube along its axis.

1. Introduction

Polymer tubes are widely used in our daily life and engineering (e.g. mechanical and biomedical fields). However, their hydrophobic nature limits the applications in many fields where good contact or even adhesion with other liquids/materials is required. For example, when these tubes are employed in biomedical engineering, the poor wettability would result in the reduction of cell attachment on their surface [1–5], which further leads to poor biocompatibility and even some critical medical accidents. In the case of bonding, low adhesion strength resulting from the poor adhesion of the surfaces [6–8] would reduce their service life and cause some hidden troubles for their applications. Therefore, surface modification of polymer tubes is of great importance before their usage. Wet chemical method and low-pressure plasma treatment are both well-known and frequently-used tools for surface modification of polymers, but the former one always involves some corrosive chemicals (e.g. trichloroisocyanuric acid solution [8] and H_2O_2/H_2SO_4 [9]) that are environmentally harmful. As an environmentally benign and effective method, low-pressure plasma exposure is widely used in polymers modification [10–13], including some works on surface modification of tube inner wall [14–16]. Plasma treatment can modify the surface properties of polymers without changing their bulk properties.

However, low-pressure plasma requires expensive vacuum equipment to create low pressure environment, which undoubtedly increases the cost and greatly limits the treated sample size and processing efficiency. In recent years, atmospheric pressure plasmas (APPs) realize the transportation of plasma from the point of generation to the point of interaction with the material [17], and thus the low-cost, easy-to-handle and efficient APPs replace low-pressure plasma to be widely used in some situations, including surface modification of polymers [18–21]. Notably, tube-APPs interaction has attracted researchers' keen interests. Tubes were widely used as a channel to transport plasma [22–26], which were further demonstrated to be a promising tool in many fields, such as biomedical applications [27–32] and surface modification [33–36]. Li et al. [34] modified the inner wall surface of quartz tube by argon/oxygen APP generated inside the tube by single needle discharge, and the results showed that the treated tube possessed better wettability. Onyshchenko et al. [35] performed hydrophilic modification of polymeric tube inner wall surface by penetrating

* Corresponding author.
E-mail address: xinliu@dlut.edu.cn (X. Liu).

http://dx.doi.org/10.1016/j.apsusc.2016.08.024
0169-4332/

atmospheric-pressure plasma jet (APPJ) into the tube. But the treatment non-uniformity of the two methods was inevitable due to the non-uniform distribution of active species along the tube. Pavlinak et al. [36] inserted a PTFE tube vertically into oxalic acid solution and filled the tube with the identical solution, and then the liquid volumes were used as electrodes to ignite surface dielectric barrier discharge at the tube surface. The generated plasma thus realized hydrophilization of PTFE tube wall surfaces. However, the above mentioned methods could not perform well in terms of treatment efficiency and application scope, especially for long tube, since the treated length would be greatly limited by the length of APPJ itself or the complexity of the discharge units. Therefore, it is urgently needed to develop an easy and high-efficient method to modify the inner walls of tubes with any length.

Actually, the key for plasma surface modification of tube inner wall is to generate or introduce plasma inside the tube. Lu et al. [37,38] found that when a helium APPJ contacted with a dielectric tube, the charges deposited on the dielectric tube wall could generate a local electric field and induce a second plasma inside the tube. Therefore, transferred atmospheric pressure plasma (TAPP), generated by directing a source plasma upon a tube filled with flowing working gas at atmospheric pressure, can be an alternative tool for the surface modification of tubes. Li et al. [39] obtained He TAPP by pointing an Ar APPJ at a tube with He flow, and found that photoionization mechanism had little effect on the generation of TAPP. They also found that when the APPJ was perpendicular to the tube, the generated TAPP had nearly equal length on both sides (i.e. the upstream and downstream) of the Ar APPJ acting point. Xiong et al. [40] further studied the mechanism of TAPP by simulations and experiments, and demonstrated that the primary ionization wave propagated across the inter-tube gap and upon impingement induced two secondary ionization waves propagating in opposite directions in the transfer tube. They also found that the preionization density was crucial for the ignition of the secondary ionization waves in the transfer tube, because a critical plasma density was required to produce sufficient space charge in the head of the ionization wave to initiate avalanche.

In this paper, we use Ar APPJ as source plasma to generate He TAPP inside a PTFE tube which is widely used in engineering but intrinsically hydrophobic, to demonstrate the great potential of TAPP for tube inner wall surface modification. The optical emission spectroscopy (OES) is used to detect the active species contained in the He TAPP. Water contact angle (WCA) measurements, atomic force microscopy (AFM) and X-ray photoelectron spectroscopy (XPS) are employed to characterize the surface modification of the tube inner wall.

2. Experimental

2.1. Materials

Transparent PTFE tubes with different outer diameters (ODs) and inner diameters (IDs) (4 mm × 3 mm, 3 mm × 2 mm, 3 mm × 1.5 mm, 2 mm × 1 mm and 1.5 mm × 0.5 mm) were purchased from Shanghai Huafang Rubber and Plastic Co. Ltd. (China).

2.2. Transferred atmospheric pressure plasma

The schematic of the experimental set-up is shown in Fig. 1. A stainless steel tube with ID of 1.4 mm and OD of 1.8 mm was inserted in a quartz tube (ID: 2.0 mm, OD: 4.0 mm) and served as both high voltage electrode and working gas channel. The stainless steel tube was flushed with argon (of purity 99.999%, Dalian Special Gases CO., LTD.), and the gas flow rate was controlled by a mass flow controller (MFC, CS200, Beijing Sevenstar Electronics

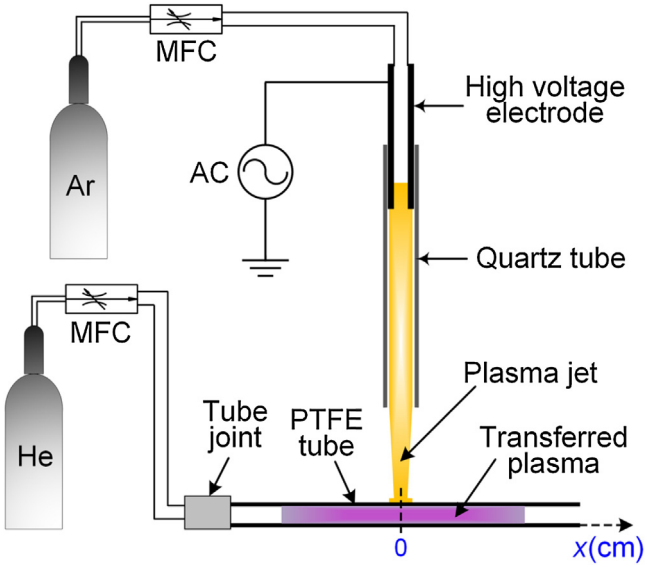

Fig. 1. Illustration of the set-up for the surface modification of PTFE tube inner wall by TAPP.

CO., LTD., China). PTFE tube was placed perpendicularly to the axis of the quartz tube, and the distance (d) between the outlet of the quartz tube and the outer wall of the PTFE tube varied from 0.5 to 1.5 cm. The PTFE tube was connected to MFC by a one-touch fitting (PG series, AirTAC Corporation in China) and was flowed with helium (of purity 99.999%, containing 1 ppm O_2 and 3 ppm H_2O, Dalian Special Gases CO., LTD.). AC power supply (Nanjing Suman Electronics, CTP–2000 K) fixed at a frequency of 60 kHz was used as driving source. After applying high enough voltage, an Ar APPJ was generated and impinged upon the PTFE tube, then He TAPP appeared inside the tube. We set the He flow direction as x axis, and the Ar APPJ impinging point was marked as 0, while the upstream and downstream were respectively labelled as positive and negative half axis.

2.3. Plasma diagnoses

The applied voltage and the discharge current were recorded by a digital oscilloscope (Tektronix TPO 2014B) with a high-voltage (HV) probe (Tektronix Tek6015A) and a current coil (Pearson 2877), respectively. The root mean square (RMS) value of applied voltage was reported in this paper. The discharge images were captured with a digital camera (Konica Minolta DiMAGE A200) to estimate the plasma length, and the exposure time was 2.0 s. The optical emission spectrum (OES) was measured by an Andor SR-750i grating monochromator (grating groove: 1200 grooves/mm, glancing wavelength: 500 nm). After the diffraction of the grating, the output spectral light could be transformed into a digital signal by CCD (Newton DU940P-BV, 100 ms exposure time) and recorded on a computer. A piece of black paper with a pinhole was carefully placed to avoid the interference from Ar APPJ while collecting the OES of He TAPP. LIFBASE developed by Luque et al. [41] was employed to calculate the rotational temperature (T_{rot}) of OH ($A^2\Sigma^+ \rightarrow X^2\Pi$) band transition. The radiant temperature profile of He TAPP was measured using an infrared thermal imager (Fluke Ti10, Fluke Inc., America).

2.4. Surface modification

For the surface modification, PTFE tubes with length of 15 cm were employed and connected to MFC. Firstly, 2.0 SLM (standard liter per minute) Ar was introduced into the stainless steel tube, and

after applied voltage was increased to 4.4 kV, an Ar APPJ generated and impinged at the center of the PTFE tube. Then when 3.0 SLM He flowed through the PTFE tube, TAPP was generated inside the tube and the plasma treatment of tube inner wall started. After 30 s plasma exposure, the plasma treatment was stopped by turning off the AC power. The time difference of every treatment was less than 0.2 s. The average power consumption P of the discharge system was obtained by the measured voltage-current waveforms and the following equation:

$$P = \frac{1}{\mathrm{T}}\int_{\mathrm{t}}^{\mathrm{t+T}} I(t)V(t)dt \quad (1)$$

where T is the period of the discharge. When the applied voltage was 4.4 kV and the PTFE tube was not flushed with He, only the Ar APPJ was ignited, and the calculated power consumption was about 3.1 W. While He flowed through the PTFE tube and TAPP was ignited, the power increased to 4.2 W. Therefore we could conclude that the power delivered to the plasma inside the tube alone was approximately 1.1 W.

2.5. Aging effect

The treated tubes were placed in an atmospheric air environment at room temperature (~25 °C) and relative humidity of 30% for more than 180 days to study their aging behavior. A constant climate chamber (DHTC-27-40-P-SD, Doaho (Shanghai) CO., LTD) was used to control the temperature and relative humidity. The fluctuations of temperature and relative humidity were less than 2 °C and 3%, respectively. The WCAs were recorded to characterize the aging behavior of the TAPP treated PTFE tubes.

2.6. Samples characterization

2.6.1. Water contact angle (WCA) measurements

The tubes were cut along its length to meet the requirements of WCA measurements, and every tube segment with a length of ~5 mm was used (e.g., the reported WCA of position $x = 0$ cm were obtained from the tube segment between $x = -0.25$ and $x = 0.25$ cm, while that of position $x = 7.5$ cm were obtained from the tube segment between $x = 7.0$ and $x = 7.5$ cm). WCAs were measured by an optical contact angle meter (Krüss, DSA100, Germany) at room temperature. The precise drop size of the used liquid was controlled by a high precision liquid microliter syringe. Deionized water droplet with a variable volume of 0.1–2.0 μL was carefully placed on the tube inner wall through the tube opening. Droplets with different volumes that could be put on the tube inner wall through the tube opening were used to estimate the influence of droplet volume on the measured WCA and was demonstrated to be negligible. Images of water droplets were then captured by a digital CCD camera (Microvision, MV-VD030SC). The profiles of the tube inner wall surface were manually detected and then the WCAs were calculated using Tangent 1 method by software (OEG GmbH SURFTENS Universal, Surftens4.3, Germany).

2.6.2. Atomic force microscopy (AFM)

The tube segments (ID = 2.0 mm) depicted above were further cut axially to obtain strips to expose their inner wall surface. Then the PTFE strip was adhered to glass slide to characterize their surface morphologies. The surface morphology and roughness of the samples were characterized by AFM (Picoplus Π, America), which was performed in tapping (non-contact) mode with a sampling range of $4 \times 4\ \mu m^2$ at the center of the strip. The root mean square (RMS) roughness was calculated by the instrument software.

2.6.3. X-ray photoelectron spectroscopy (XPS)

The surface chemical compositions of the tubes (ID = 2.0 mm) were analyzed by XPS, and the tube strips were used as test samples. XPS spectra were recorded by Thermo ESCALAB 250Xi instrument equipped with a monochromatic Al Kα X-ray beam ($h\nu = 1486.6$ eV). The power of this source was set to 150 W and the beam was focused at the center of the strip. Survey scans and high-resolution C 1s peaks were recorded at a take-off angle of 45 ° relative to the sample surface. The pass energy and energy step of survey scans were respectively 70.0 and 1.0 eV, while those of C 1s individual high-resolution spectra were respectively 30.0 and 0.05 eV. The binding energy of C 1s in hydrocarbon (284.6 eV) was used as calibration reference. High-resolution C 1 s spectra were deconvoluted into different carbon-containing chemical groups with mixed Lorentzian–Gaussian components by XPS Peak v4.1 fitting software. A Shirley-type background subtraction was used and the full-width at half maximum (FWHM) of each line-shape was allowed to vary from 1.4 to 2.2 eV for the untreated surfaces and from 1.2 to 2.0 eV for the plasma treated surfaces.

3. Results and discussion

3.1. He TAPP discharge images

Fig. 2(a) shows the side view of TAPP generated in PTFE tube (ID = 2.0 mm) at various applied voltages. The TAPP lengths in upstream and downstream both significantly increased with the applied voltage, which was consistent with the results of Li et al. [39]. Additionally, the luminous intensity of Ar APPJ and He TAPP increased with the applied voltage. When the applied voltage increased, the Ar discharge was directly enhanced, resulting in obviously strengthened emission intensity and charge deposition on the PTFE tube wall. Therefore, an increased magnitude of the electric field across the PTFE tube wall formed and thus the plasma length and emission intensity of the TAPP increased. Fig. 2(b) shows the length of TAPP as a function of Ar and He gas flow rate when applied voltage was 4.0 kV. When Ar flow rate was fixed at 2.0 SLM, the plasma length increased with He flow rate and reached its maximum at 5.0 SLM, after which gradually decreased due to the transition from a laminar to turbulent flow [42]. Similarly, when He flow rate was fixed at 3.0 SLM, the TAPP length firstly increased and peaked at 2.0 SLM and then continuously decreased. This could be attributed to the change of discharge characteristics of Ar APPJ due to the heat removal by increased Ar gas flow [43], which further caused the reduction of charge deposited on the PTFE tube wall. As a result, the induced local electric field was weakened and the plasma length decreased. The experiments reported below were all conducted by fixing Ar and He flow rates at 2.0 and 3.0 SLM, respectively. Fig. 2(c) shows the influence of distance (d) between the outlet of the quartz tube and the outer wall of the PTFE tube on TAPP at applied voltages of 3.0 and 3.5 kV. It could be clearly seen that d had an obvious impact on TAPP, and the smaller d the longer TAPP. When applied voltage was 3.0 kV, the TAPP with $d = 0.5$ cm was about 12 cm long while that with $d = 1.5$ cm was almost invisible. Fig. 2(d) illustrates the discharge images of TAPP in tubes with different ID (left) at applied voltage of 3.5 kV, and the corresponding magnified images on the right were taken from the same positions shown in the yellow dashed boxes. When the tube ID increased from 0.5 to 3.0 mm, the TAPP length decreased from ~21 to ~7 cm, and the luminous intensity of the TAPP also gradually decreased, which demonstrated that the TAPP was greatly influenced by the tube ID: the smaller ID, the longer TAPP and the stronger discharge inside the tube.

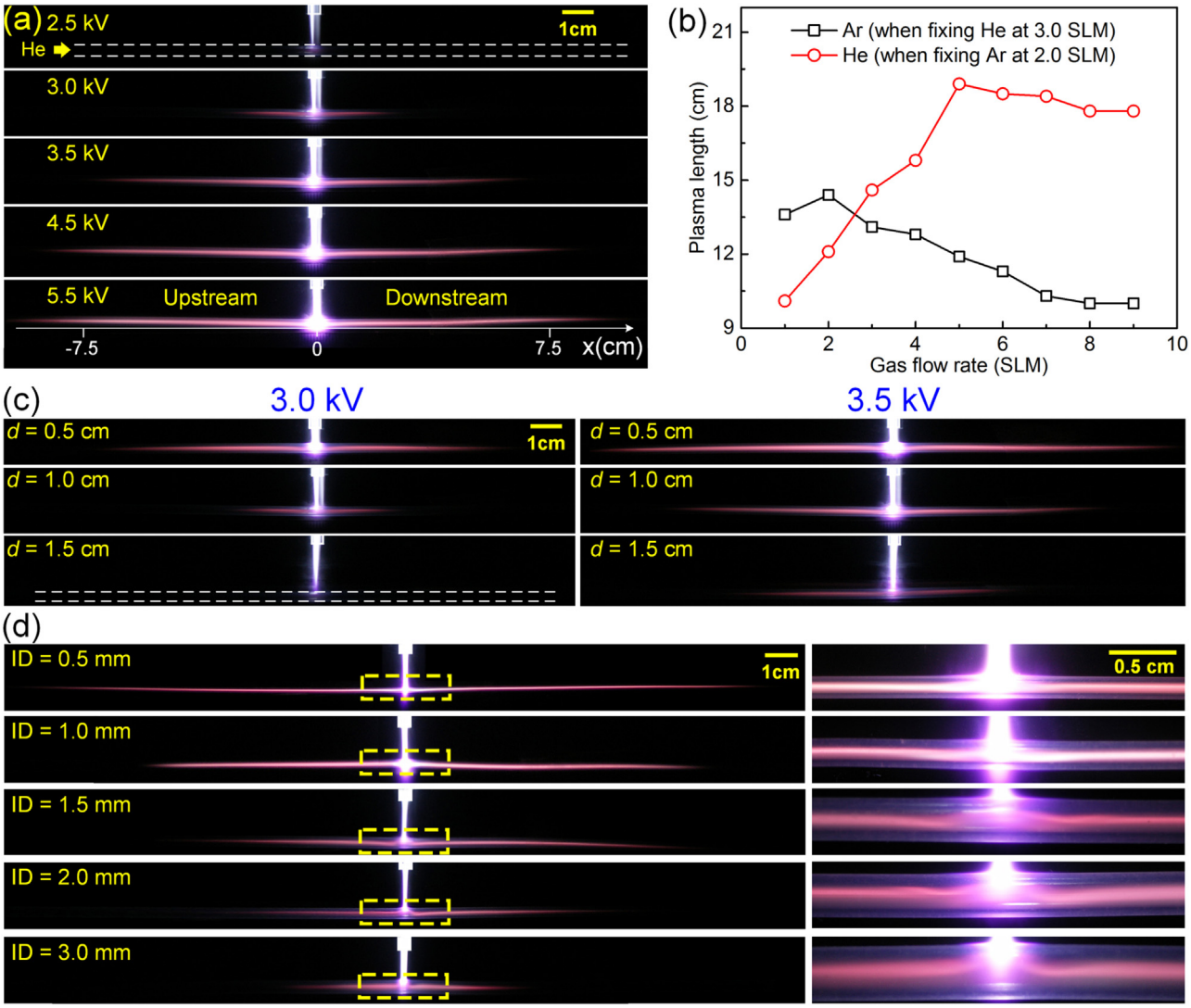

Fig. 2. (a) Side views of TAPP inside a PTFE tube (ID = 2.0 mm) under different applied voltage; (b) the influence of Ar and He gas flow on the TAPP length; (c) The influence of *d* on TAPP at applied voltages of 3.0 and 3.5 kV; (d) The discharge images of TAPP in tubes with different ID (left) at applied voltage of 3.5 kV, the corresponding magnified images (right) were taken from the same positions shown in the yellow dashed boxes. (For interpretation of the references to colour in this figure legend, the reader is referred to the web version of this article.)

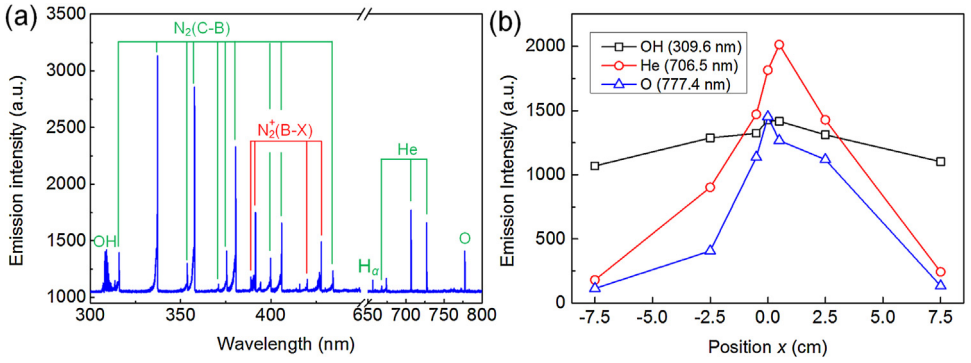

Fig. 3. (a) Typical OES of He TAPP and (b) the emission intensity of OH($A^2\Sigma^+ \rightarrow X^2\Pi$, 309.6 nm), He($3s^3S \rightarrow 2p^3P$, 706.5 nm) and O($3p^5P \rightarrow 3s^5S$, 777.4 nm) in the He TAPP at different positions of the PTFE tube.

3.2. OES and plasma gas temperature

Fig. 3(a) shows the typical OES of He TAPP at $x = 0$ with the wavelength range between 300 and 800 nm. The OES spectrum in the range of 300–450 nm were dominated by the vibration transitions of $N_2(C^3\Pi_u \rightarrow B^3\Pi_g)$ and N+ $2(B^2\Sigma + u \rightarrow X^2\Sigma + g)$. We observed intensive He emission lines at 667.9, 706.6 and 728.1 nm from excited He atoms which could be produced by electron-

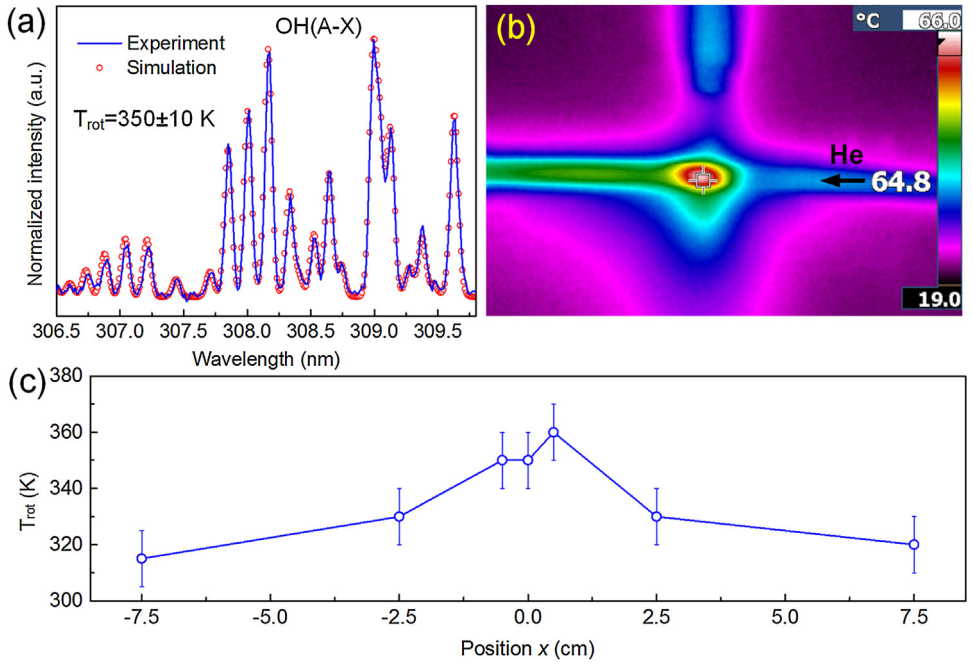

Fig. 4. (a) Experimental and simulated spectra of OH($A^2\Sigma^+ \rightarrow X^2\Pi$) band transition from 306.5 to 309.8 nm; (b) the thermographic images of the He TAPP; (c) the T_{rot} of the He TAPP at different positions of the PTFE tube.

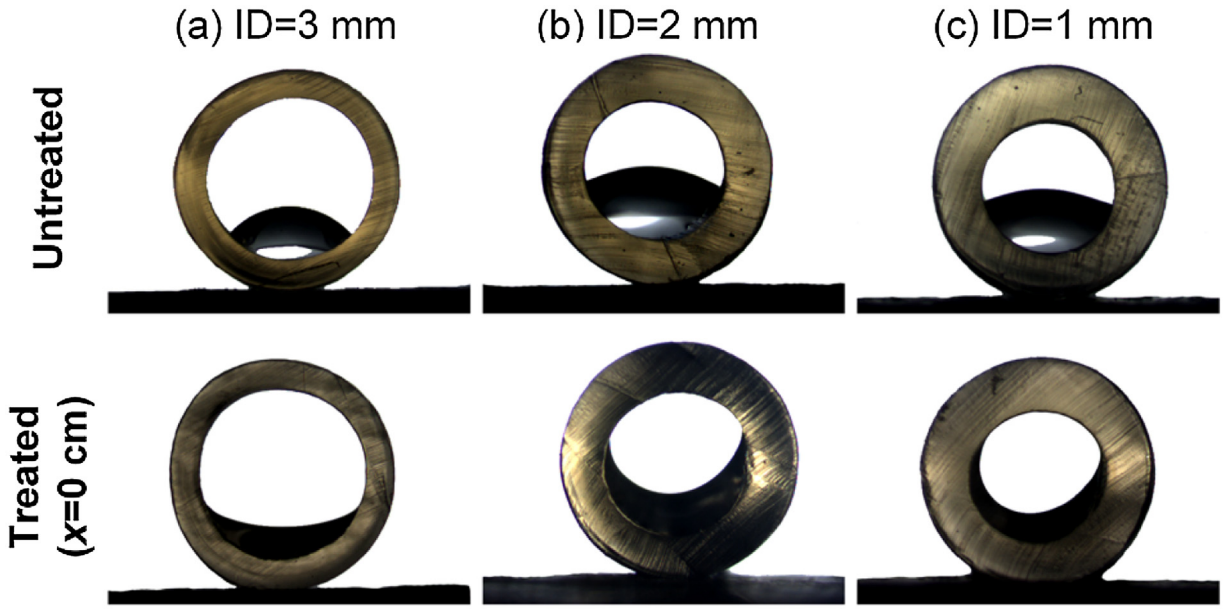

Fig. 5. Images of water droplets on inner wall of untreated and treated tubes with different IDs: (a) ID = 3 mm, (b) ID = 2 mm and (c) ID = 1 mm.

impact reactions and ion-electron recombination [44]. In addition, some UV radiation observed from the spectra at approximately 306–310 nm can be referenced to the emission of OH($A^2\Sigma^+ \rightarrow X^2\Pi$) band transition. Hα at 656.3 nm and atomic O at 777.4 nm were also detected. The presence of these radicals in He TAPP was due to the direct electron impact dissociation or excitation transfer reactions of a small amount of impurities (e.g. H_2O molecule, nitrogen and oxygen) in the feed gas and on the tube wall of the gas delivery system or diffusion through the tube [45,46]. Therefore, it was evident that the He TAPP contained many active species and offered high plasma chemical activity, and these radicals could play important roles in applications such as surface modification and biomedicine. Fig. 3(b) depicts the emission intensities of OH($A^2\Sigma^+ \rightarrow X^2\Pi$, 309.6 nm), He($3s^3S \rightarrow 2p^3P$, 706.5 nm) and O($3p^5P \rightarrow 3s^5S$, 777.4 nm) in the He TAPP at different positions of the PTFE tube. It clearly shows that the emission intensity of these species peaked around the position $x = 0$ cm, while gradually decreased along the two directions.

As an important parameter of gas discharge plasma, rotational temperature (T_{rot}) is always obtained by comparison between experimental data and theoretical spectrum of OH($A^2\Sigma^+ \rightarrow X^2\Pi$) emission bands [47–50]. Fig. 4(a) depicts the experimental data ($x = 0$ cm) and simulated spectra of the OH($A^2\Sigma^+ \rightarrow X^2\Pi$) band from 306.5 to 309.8 nm, indicating that the T_{rot} of He TAPP at the position of $x = 0$ cm was about 350 ± 10 K. Gas temperature is one of the most important parameters for plasma applications,

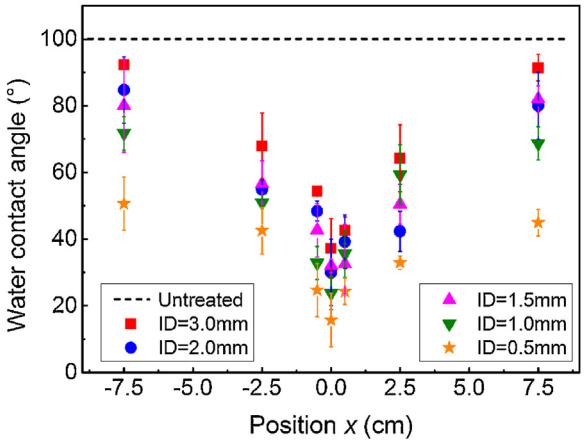

Fig. 6. WCAs of different positions on the inner wall surface of treated PTFE tube with different IDs.

which can be roughly estimated by T_{rot}, because T_{rot} is always considered to be equal to the gas temperature of APPs [51,52]. However, some recent works demonstrated that the T_{rot} determined by OH($A^2\Sigma^+ \rightarrow X^2\Pi$) band was much higher than the measured plasma gas temperature due to the overpopulation of high rotational states of OH($A^2\Sigma^+$) [49,50]. So we employed thermal imaging analysis to map the plasma gas temperature profile of He TAPP, and the result was shown in Fig. 4(b). The thermographic images clearly indicated that the temperature of He TAPP at position of $x = 0$ cm was about 64.8 °C (~338 K), which was close to the simulated results in Fig. 4(a). Therefore, T_{rot} obtained from spectra-fitting could be used to roughly estimate the gas temperature of TAPP in our study. The T_{rot} at different positions along He TAPP are shown in Fig. 4(c), from which one could clearly see that the temperature maximized at the position around $x = 0$ cm (~350 K) and gradually decreased along the two directions to nearly 320 ± 10 K. This also demonstrated that the TAPP inside the tube had a low temperature, so the TAPP was an excellent candidate for surface modification of tubes, especially for those made of heat-sensitive materials.

3.3. WCA measurements

During the surface modification, the center of PTFE tube was fixed at $x = 0$ cm (Fig. 2(a)), while the gas inlet and outlet were respectively at $x = -7.5$ and 7.5 cm. Fig. 5 shows the images of the water droplets on inner wall ($x = 0$ cm) of untreated and treated tubes with ID of 3, 2 and 1 mm, and the volume of the used water droplets were respectively 2.0, 1.5 and 0.3 μL. The WCAs of these untreated tube inner walls at the position of $x = 0$ cm were about $100 \pm 2°$, and the values decreased to $28 \pm 10°$ after TAPP treatment for 30 s, which clearly exhibited enhanced hydrophilicity upon plasma treatment.

Fig. 6 depicts the WCAs of different positions on the inner wall surface of treated PTFE tubes with different IDs. It clearly shows that the treatment was lengthwise non-uniform and the wettability improved the most at the position $x = 0$ cm for all tubes, and the improvement degree gradually decreased along two directions. This can be explained by the distribution of reactive species along the whole PTFE tube, as shown in Fig. 3. Since the emission intensities of these species peaked around $x = 0$ cm and then decreased towards the two directions, the treatment effect was therefore weakened as the distance to $x = 0$ increased. However, when the PTFE tube was moved along its axial direction, uniform hydropholicity could be obtained for tubes with any length. Fig. 6 also indicates that the lowest WCA was found on the surface of tube with smallest ID (0.5 mm) and that the WCAs at a similar position tended to rise with increasing ID. Therefore a better modification efficiency was obtained for the tubes with smaller ID. According to the results obtained by both simulations an d experiments, for the plasma generated inside a tube, the decrease of tube ID results in the increase of average electron density and the number density of reactive species [53–56], Fig. 2(d) also demonstrated that the discharge intensity in tube with smaller ID was more intense, so tube with smaller ID experienced more intense surface modification in our conditions.

3.4. Surface morphology and roughness

Fig. 7 shows the typical 2D AFM images and RMS roughness of inner wall surfaces of untreated and treated PTFE tube (ID = 2.0 mm) at different positions. For the original PTFE tube, the inner wall surface shown in Fig. 7(a) was characterized by some stripy textures, which may be formed during manufacture, and the RMS roughness was 16.24 ± 6.38 nm. After TAPP exposure for 30 s, the perthitic features were greatly reduced and the surfaces became smooth and uniform. The RMS roughness of the plasma treated inner wall surfaces decreased after TAPP treatment for 30 s. Most obviously, at the position of $x = 0$ cm, where the induced discharge was the most intense and the reactive species were the richest (Fig. 3), the lowest roughness of 5.47 ± 0.32 nm could be seen.

Both the chemically reactive species and the non-reactive but energetic species (e.g. photons, electrons, non-reactive ions and non-reactive excited species) are responsible for plasma etching (including physical sputtering and chemical etching) under atmospheric pressure [18,57]. During our surface modification of PTFE, He metastables and reactive O atoms were undoubtedly responsible for the scission of $-(CF_2)_n-$ chains and the subsequent surface modification. Helium metastables are highly energetic species (e.g., the energy of 2^3S and 2^1S helium states are respectively 19.82 and 20.62 eV), so they can easily break organic bonds, such as C—C (3.8 eV) and C–F (4.7 eV). O can easily react chemically with the polymer (selective chemical etching or oxygen-containing groups' introduction) creating surface modifications. According to the previous studies about plasma treatment of PTFE [57–60], O_2-free plasmas treatment was dominated by physical etching without any preferential orientation and always resulted in a hydrophilic surface, while O_2-containing plasmas exposure was mainly accompanied by selective chemical etching of the amorphous phase and usually increased the roughness and obtained (super)hydrophobic surface. Under our experimental conditions, the treated PTFE tube inner wall became hydrophilic and smoother in comparison with the untreated one, we could conclude that the selective chemical etching was negligible.

3.5. Surface chemical composition

Fig. 8 shows the XPS spectra of untreated inner wall surface and treated one at different positions. It can be easily found that the surfaces were all composed of elements F, O, N and C with different relative contents (at.%). The relative contents of F and O for the untreated tube inner wall surface were respectively 70.71 and 0.38 at.%. But the amount of these elements changed after He TAPP treatment, especially at the positions of $x = 0$ and ±0.5 cm, as shown in Fig. 8(b). At the position of $x = 0$ cm of the treated tube inner wall, the amount of O increased to 8.41 at.%, while the F content significantly decreased to 50.49 at.%. For other positions of the treated tube inner wall, though the F (O) increased (decreased) along each direction in comparison with $x = 0$ cm, the content of F (O) was lower (larger) than that of the untreated tube inner wall. Therefore we can conclude that the surface wettability change of the tube inner wall agreed well with the surface F and O distribution along the tube, which was consistent with the study of D. Pavlinak et al. [36], who

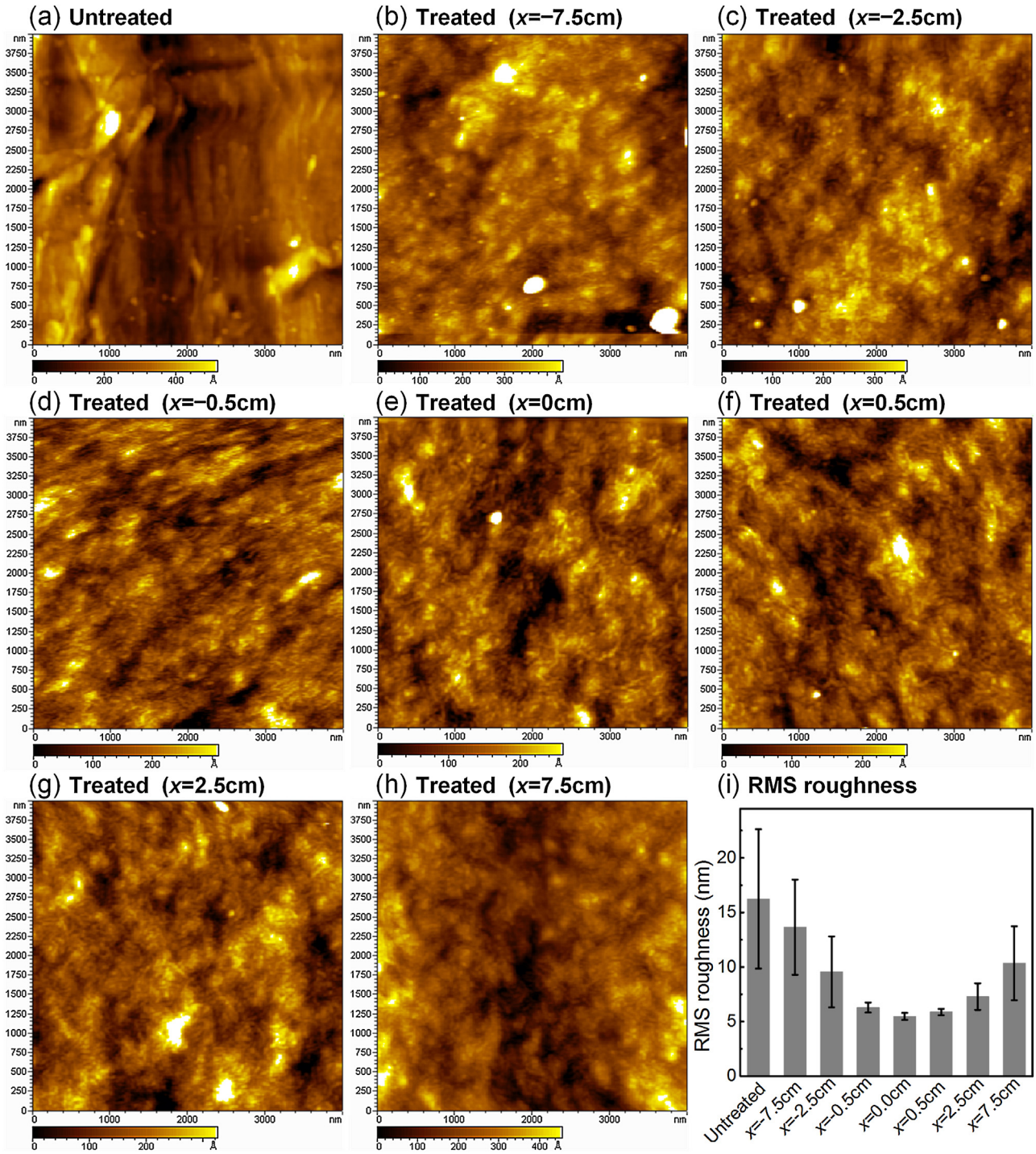

Fig. 7. Typical 2D AFM images (a)-(h) and RMS roughness (i) of inner wall surfaces of untreated and treated tubes (ID = 2.0 mm).

found that the replacement of surface F by O was responsible for the wettability improvement of plasma treated PTFE surface.

High-resolution C 1s XPS peak fitting was performed to investigate the change of surface chemical groups in detail. Fig. 9(a)–(h) shows the peak-fitted C 1 s XPS spectra for untreated and treated inner wall surfaces at different positions. The C 1s spectra were deconvoluted into seven components [61,62]: C—C/C—H peak centered at 284.7 ± 0.1 eV, C—O/C—OH/C—CF group at 286.1 ± 0.1 eV, C═O/O—C—O component at 287.3 ± 0.1 eV, O—C═O/COOH group at 288.8 ± 0.1 eV, —CF at 290.0 ± 0.2 eV, $-CF_2$/–CF–O moiety at 291.8 ± 0.5 eV and $-CF_3$/$-CF_2$—O group at 293.5 ± 0.5 eV. The relative concentrations (%) of the fitted chemical groups are shown in Table 1. According to the results present in Fig. 9(a)–(h) and Table 1, the original inner wall surface was dominated by fluorine containing groups, which determined its natural hydrophobicity. After He TAPP treatment, the contents of fluorine containing groups decreased while oxygen containing groups increased, especially at the position of $x = 0$ cm where saw the most fluorine containing groups decrease and oxygen containing groups increase. Fig. 9(i) shows the high-resolution O 1s XPS spectra for untreated and treated inner wall surfaces, which clearly demonstrated that the O 1s peak intensity reached its maximum at $x = 0$ cm and decreased

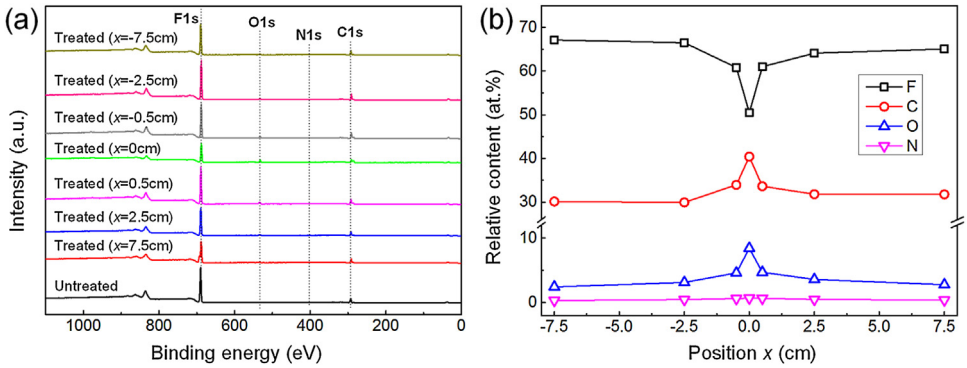

Fig. 8. (a) XPS spectra and (b) element relative contents of untreated and treated inner wall surfaces (ID = 2.0 mm).

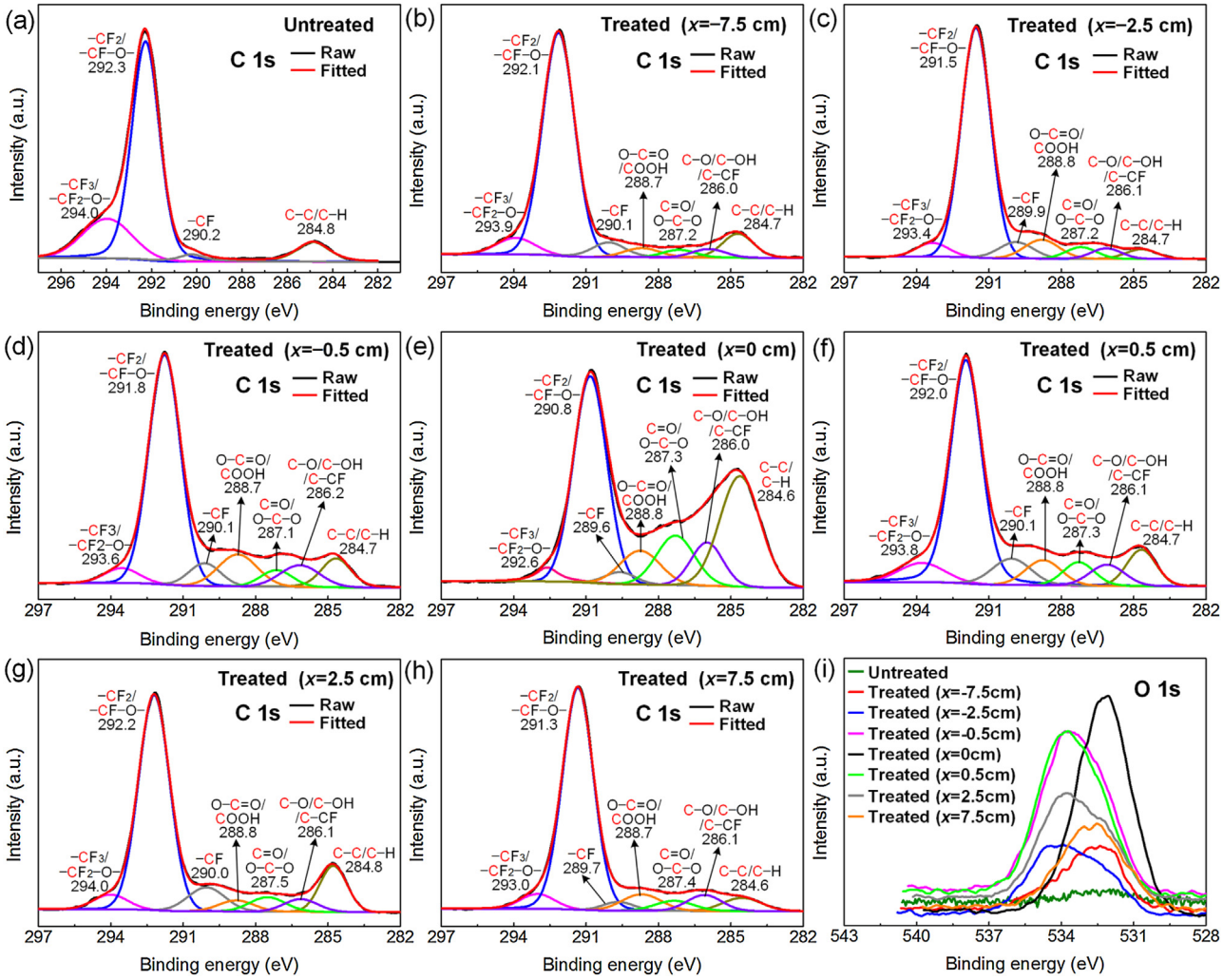

Fig. 9. (a)–(h) Peak-fitted high-resolution C 1 s XPS spectra and (i) high-resolution O 1s XPS spectra for untreated and treated inner wall surfaces at different positions.

Table 1
The relative concentrations (%) of the peaks for C 1 s of untreated and treated inner wall surfaces.

Moieties	Binding energy(eV)	Untreated	Treated (x (cm))						
			−7.5	−2.5	−0.5	0.0	0.5	2.5	7.5
C—C/C—H	284.7 ± 0.1	5.6	8.7	5.2	8.1	22.1	8.3	10.7	6.6
C—O/C—OH/C—CF	286.1 ± 0.1	0	2.8	3.4	2.2	8.2	5.9	4.0	5.5
C=O/O—C—O	287.3 ± 0.1	0	2.5	4.1	4.6	11.2	5.9	4.8	4.3
O—C=O/COOH	288.8 ± 0.1	0	3.2	7.9	10.8	10.5	8.9	6.6	5.2
–CF	290.0 ± 0.2	3.9	5.4	6.0	6.2	4.2	5.9	6.3	3.7
$-CF_2$/—CF—O	291.8 ± 0.5	68.3	70.2	67.3	63.6	41.0	58.4	63.0	68.4
$-CF_3$/—CF_2—O	293.5 ± 0.5	22.2	7.2	6.1	4.5	2.8	6.7	4.6	6.3

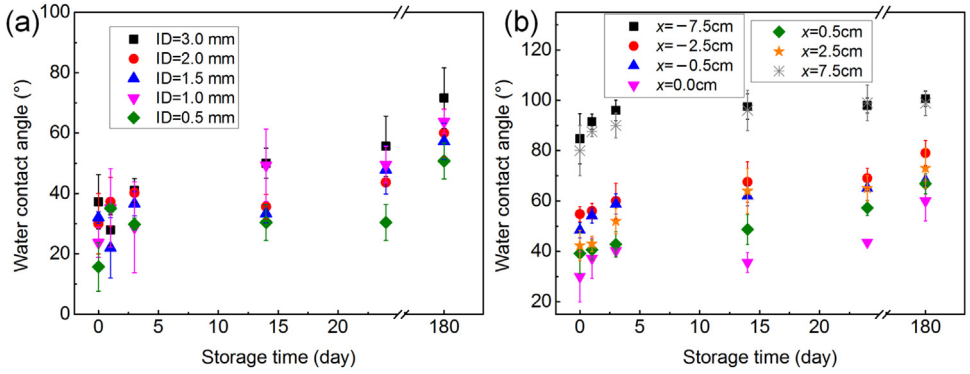

Fig. 10. Aging effect of the treated PTFE tube inner wall during 180 days: (a) tubes with different ID at $x = 0$ cm and (b) tube with ID of 2.0 mm at different positions x.

along two directions, but the intensities were all higher than that of untreated surface. As we know, fluorine (oxygen) containing groups represent low (high) surface energy, which is crucial for surface hydrophobicity (hydrophilicity). Therefore, the decrease of fluorine containing groups and increase of oxygen containing groups contributed to the improved wettability of PTFE tube inner wall after TAPP treatment.

3.6. Aging effect

Stability of plasma-induced hydrophilicity is always an important issue, because the treated surface always recover its original wettability (i.e. aging effect) [63–66]. After plasma exposure, the treated surface tends to reorganize in order to minimize its energy and return to equilibrium. Some mechanisms, including reorientation of modified chemical groups into the bulk, diffusion of non-modified species from the bulk to the top layer and adsorption of organic contaminants from air, are supposed to be responsible for aging behavior. The WCAs of the treated tubes during 180 days' aging were recorded and plotted in Fig. 10. Results shown in Fig. 10(a) present the WCAs at $x = 0$ cm of treated tubes with different IDs as a function of storage time. It clearly indicated that the WCAs at $x = 0$ cm increased slightly during the storage, especially for the tube with smaller ID, and that the treated PTFE tubes retained its hydrophilicity at this position even after 180 days' storage. Fig. 10(b) illustrates the aging effect of different positions on treated tube with ID of 2.0 mm, and it shows that the aging speeds of surfaces at $x = 0$, ± 0.5 and ± 2.5 cm were much slower than that of the ones at $x = \pm 7.5$ cm, demonstrating that the more intense surface modification, the better wettability stability, because the polymer chain reorientations were retarded for the deeply modified one [67].

4. Conclusions

In summary, we reported hydrophilization of tube inner wall by TAPP. Illustrated herein was surface modification of PTFE tube inner wall by He TAPP inside the tube induced by an Ar APPJ. Results demonstrated that the wettability of the tube inner wall was improved by both plasma etching and plasma oxidation. The surface modification and the subsequent aging exhibited some non-uniformity along the PTFE tube, which was originated from the inhomogeneity of active species contained by the He TAPP. The improvement and stability of the wettability around the position of $x = 0$ cm were much better than those of other positions. However, we could easily realize a homogeneous and long-lasting TAPP treatment on the inner wall surface of tube with any length via feeding the tube along its axis. This could overcome the challenge that previous works faced [34–36]. Furthermore, TAPP could have great application potentials in surface engineering and biomedical fields of tubes and other hollow bodies, such as tube inner wall cleaning and less invasive plasma triggered endoscopy [68].

Acknowledgements

This work was financially supported by National Basic Research Program of China (Grant No. 2015CB057304), National Natural Science Foundation of China (Grant No. 51305060 and 51275072) and the Fundamental Research Funds for the Central Universities (Grant No.DUT15RC(4)21).

References

[1] R.A. D'Sa, G.A. Burke, B.J. Meenan, Protein adhesion and cell response on atmospheric pressure dielectric barrier discharge-modified polymer surfaces, Acta Biomater. 6 (2010) 2609–2620.
[2] K.G. Doherty, J. Oh, P. Unsworth, A. Bowfield, C.M. Sheridan, P. Weightman, J.W. Bradley, R.L. Williams, Polystyrene surface modification for localized cell culture using a capillary dielectric barrier discharge atmospheric-Pressure microplasma jet, Plasma Process Polym. 10 (2013) 978–989.
[3] I. Trizio, F. Intranuovo, R. Gristina, G. Dilecce, P. Favia, He/O-2 atmospheric pressure plasma jet treatments of PCL scaffolds for tissue engineering and regenerative medicine, Plasma Process Polym. 12 (2015) 1451–1458.
[4] A.K. Riau, D. Mondal, G.H.F. Yam, M. Setiawan, B. Liedberg, S.S. Venkatraman, J.S. Mehta, Surface modification of PMMA to improve adhesion to corneal substitutes in a synthetic core-Skirt keratoprosthesis, Acs Appl. Mater. Int. 7 (2015) 21690–21702.
[5] F. Rezaei, B. Shokri, M. Sharifian, Atmospheric-pressure DBD plasma-assisted surface modification of polymethyl methacrylate: a study on cell growth/proliferation and antibacterial properties, Appl. Surf. Sci. 360 (2016) 641–651.
[6] J. Schaefer, T. Hofmann, J. Holtmannspoetter, M. Frauenhofer, J. von Czarnecki, H. Gudladt, Atmospheric-pressure plasma treatment of polyamide 6 composites for bonding with polyurethane, J. Adhes Sci. Technol. 29 (2015) 1807–1819.
[7] J.A. Juarez-Moreno, A. Avila-Ortega, A.I. Oliva, F. Aviles, J.V. Cauich-Rodriguez, Effect of wettability and surface roughness on the adhesion properties of collagen on PDMS films treated by capacitively coupled oxygen plasma, Appl. Surf. Sci. 349 (2015) 763–773.
[8] M.D. Romero-Sanchez, M.M. Pastor-Blas, J.M. Martin-Martinez, Adhesion improvement of SBR rubber by treatment with trichloroisocyanuric acid solutions in different esters, Int J. Adhes Adhes 21 (2001) 325–337.
[9] C. Lohbach, U. Bakowsky, C. Kneuer, D. Jahn, T. Graeter, H.J. Schafers, C.M. Lehr, Wet chemical modification of PTFE implant surfaces with a specific cell adhesion molecule, Chem. Commun. (2002) 2568–2569.
[10] E.M. Liston, L. Martinu, M.R. Werthtimer, Plasma surface modification of polymers for improved adhesion: a critical review, J. Adhes Sci. Technol. 7 (1993) 1091–1127.
[11] T. Desmet, R. Morent, N. De Geyter, C. Leys, E. Schacht, P. Dubruel, Nonthermal plasma technology as a versatile strategy for polymeric biomaterials surface modification: a review, Biomacromolecules 10 (2009) 2351–2378.
[12] K.N. Pandiyaraj, R.R. Deshmukh, A. Arunkumar, M.C. Ramkumar, I. Ruzybayev, S.I. Shah, P. Su, M.H. Periayah, A.S. Halim, Evaluation of mechanism of non-thermal plasma effect on the surface of polypropylene films for enhancement of adhesive and hemo compatible properties, Appl. Surf. Sci. 347 (2015) 336–346.
[13] O.V. Penkov, M. Khadem, W. Lim, D. Kim, A review of recent applications of atmospheric pressure plasma jets for materials processing, J. Coat. Technol. Res. 12 (2015) 225–235.

[14] J.L. Lauer, J.L. Shohet, R.M. Albrecht, S. Esnault, J.S. Malter, U.H. von Andrian, S.B. Shohet, Control of uniformity of plasma-surface modification inside of small-diameter polyethylene tubing using microplasma diagnostics, Ieee T, Plasma Sci. 33 (2005) 791–798.
[15] J. Pollak, M. Moisan, D. Keroack, J. Seguin, J. Barbeau, Plasma sterilisation within long and narrow bore dielectric tubes contaminated with stacked bacterial spores, Plasma Process Polym. 5 (2008) 14–25.
[16] Y.K. Cho, D. Park, H. Kim, H. Lee, H. Park, H.J. Kim, D. Jung, Bioactive surface modifications on inner walls of poly-tetra-fluoro-ethylene tubes using dielectric barrier discharge, Appl. Surf. Sci. 296 (2014) 79–85.
[17] X. Lu, G.V. Naidis, M. Laroussi, S. Reuter, D.B. Graves, K. Ostrikov, Reactive species in non-equilibrium atmospheric-pressure plasmas: generation, transport, and biological effects, Phys. Rep. 630 (2016) 1–84.
[18] S.A. Rich, T. Dufour, P. Leroy, L. Nittler, J.J. Pireaux, F. Reniers, Low-density polyethylene films treated by an atmospheric Ar-O 2 post-discharge: functionalization, etching, degradation and partial recovery of the native wettability state, J. Phys. D: Appl. Phys. 47 (2014) 65203.
[19] E.C. Preedy, S. Perni, P. Prokopovich, Nanomechanical and surface properties of rMSCs post-exposure to CAP treated UHMWPE wear particles, Nanomed.: NBM 12 (2016) 723–734.
[20] I. Onyshchenko, A.Y. Nikiforov, N. De Geyter, R. Morent, Local analysis of pet surface functionalization by an atmospheric pressure plasma jet, Plasma Process Polym. 12 (2015) 466–476.
[21] A. Sarani, A.Y. Nikiforov, N. De Geyter, R. Morent, C. Leys, Surface modification of polypropylene with an atmospheric pressure plasma jet sustained in argon and an argon/water vapour mixture, Appl. Surf. Sci. 257 (2011) 8737–8741.
[22] V. Sarron, E. Robert, S. Dozias, M. Vandamme, D. Ries, J.M. Pouvesle, Splitting and mixing of high-Velocity ionization-Wave-Sustained atmospheric-Pressure plasmas generated with a plasma gun, ieee t, Plasma Sci. 39 (2011) 2356–2357.
[23] K.G. Kostov, M. Machida, V. Prysiazhnyi, R.Y. Honda, Transfer of a cold atmospheric pressure plasma jet through a long flexible plastic tube, Plasma Sour. Sci. Technol. 24 (2015) 25038.
[24] F. Clement, P. Svarnas, L. Marlin, A. Gkelios, B. Held, Atmospheric-Pressure plasma microjet of Argon?Nitrogen mixtures directed by dielectric flexible tubes, ieee t, Plasma Sci. 39 (2011) 2364–2365.
[25] C. Monge-Dauge, F. Clement, P. Svarnas, J. Loiseau, A. Ricard, B. Held, Experimental study coupled with electrical modeling for the consideration of DBD-Based plasma jet, ieee t, Plasma Sci. 40 (2012) 2254–2260.
[26] Z. Xiong, E. Robert, V. Sarron, J. Pouvesle, M.J. Kushner, Dynamics of ionization wave splitting and merging of atmospheric-pressure plasmas in branched dielectric tubes and channels, J. Phys. D: Appl. Phys. 45 (2012) 275201.
[27] K.G. Kostov, T.M.C. Nishime, M. Machida, A.C. Borges, V. Prysiazhnyi, C.Y. Koga-Ito, Study of cold atmospheric plasma jet at the end of flexible plastic tube for microbial decontamination, Plasma Process Polym. 12 (2015) 1383–1391.
[28] Z. Kovalova, M. Leroy, C. Jacobs, M.J. Kirkpatrick, Z. Machala, F. Lopes, C.O. Laux, M.S. DuBow, E. Odic, Atmospheric pressure argon surface discharges propagated in long tubes: physical characterization and application to bio-decontamination, J. Phys. D: Appl. Phys. 48 (2015) 464003.
[29] P. Svarnas, S.H. Matrali, K. Gazeli, S. Aleiferis, F. Clement, S.G. Antimisiaris, Atmospheric-pressure guided streamers for liposomal membrane disruption, Appl. Phys. Lett. 101 (2012) 264103.
[30] M. Polak, J. Winter, U. Schnabel, J. Ehlbeck, K. Weltmann, Innovative plasma generation in flexible biopsy channels for inner-tube decontamination and medical applications, Plasma Process Polym. 9 (2012) 67–76.
[31] A. Pointu, A. Ricard, E. Odic, M. Ganciu, Nitrogen atmospheric pressure post discharges for surface biological decontamination inside small diameter tubes, Plasma Process Polym. 5 (2008) 559–568.
[32] H. Eto, Y. Ono, A. Ogino, M. Nagatsu, Low-temperature internal sterilization of medical plastic tubes using a linear dielectric barrier discharge, Plasma Process Polym. 5 (2008) 269–274.
[33] W. Huang, S. Li, Preliminary study on applications of an atmospheric-Pressure argon plasma discharge with a single-electrode configuration, ieee t, Plasma Sci. 38 (2010) 121–126.
[34] S. Li, W. Huang, J. Zhang, D. Wang, Optical diagnosis of an argon/oxygen needle plasma generated at atmospheric pressure, Appl. Phys. Lett. 94 (2009) 111501.
[35] I. Onyshchenko, N. De Geyter, A.Y. Nikiforov, R. Morent, Atmospheric pressure plasma penetration inside flexible polymeric tubes, Plasma Process Polym. 12 (2015) 271–284.
[36] D. Pavliňák, O. Galmiz, M. Zemánek, A. Brablec, J. Čech, M. Černák, Permanent hydrophilization of outer and inner surfaces of polytetrafluoroethylene tubes using ambient air plasma generated by surface dielectric barrier discharges, Appl. Phys. Lett. 105 (2014) 154102.
[37] X. Lu, Q. Xiong, Z. Xiong, J. Hu, F. Zhou, W. Gong, Y. Xian, C. Zou, Z. Tang, Z. Jiang, Y. Pan, Propagation of an atmospheric pressure plasma plume, J. Appl. Phys. 105 (2009) 43304.
[38] X. Lu, G.V. Naidis, M. Laroussi, K. Ostrikov, Guided ionization waves: theory and experiments, Phys. Rep. 540 (2014) 123–166.
[39] S. Li, W. Huang, D. Wang, An atmospheric-pressure helium plasma jet induced by an atmospheric-pressure argon plasma discharge in a single-electrode configuration, Ieee T, Plasma Sci. 37 (2009) 1825–1829.
[40] Z. Xiong, E. Robert, V. Sarron, J. Pouvesle, M.J. Kushner, Atmospheric-pressure plasma transfer across dielectric channels and tubes, J. Phys D Appl Phys 46 (2013) 155203.
[41] J. Luque, D.R. Crosley, LIFBASE: Database and spectral simulation, SRI international report MP 99 (1999).
[42] Q. Li, J. Li, W. Zhu, X. Zhu, Y. Pu, Effects of gas flow rate on the length of atmospheric pressure nonequilibrium plasma jets, Appl. Phys. Lett. 95 (2009) 141502–141503.
[43] S. Li, W. Huang, D. Wang, The effect of gas flow on argon plasma discharge generated with a single-electrode configuration at atmospheric pressure, Phys. Plasmas 16 (2009) 93501.
[44] D.X. Liu, P. Bruggeman, F. Iza, M.Z. Rong, M.G. Kong, Global model of low-temperature atmospheric-pressure He + H2O plasmas, Plasma Sour. Sci. Technol. 19 (2010) 25018.
[45] A. Schmidt-Bleker, S.A. Norberg, J. Winter, E. Johnsen, S. Reuter, K.D. Weltmann, M.J. Kushner, Propagation mechanisms of guided streamers in plasma jets: the influence of electronegativity of the surrounding gas, Plasma Sour. Sci. Technol. 24 (35022) (2015).
[46] J. Winter, K. Wende, K. Masur, S. Iseni, M. Duennbier, M.U. Hammer, H. Tresp, K. Weltmann, S. Reuter, Feed gas humidity: a vital parameter affecting a cold atmospheric-pressure plasma jet and plasma-treated human skin cells, J. Phys. D: Appl. Phys. 46 (2013) 295401.
[47] S. Pellerin, J.M. Cormier, F. Richard, K. Musiol, J. Chapelle, A spectroscopic diagnostic method using UV OH band spectrum, J. Phys. D: Appl. Phys. 29 (1996) 726–739.
[48] Q. Xiong, A.Y. Nikiforov, M.A. Gonzalez, C. Leys, X.P. Lu, Characterization of an atmospheric helium plasma jet by relative and absolute optical emission spectroscopy, Plasma Sour. Sci. Technol. 22 (2013) 15011.
[49] S. Wu, X. Lu, D. Zou, Y. Pan, Effects of H-2 on Ar plasma jet: from filamentary to diffuse discharge mode, J. Appl. Phys. 114 (2013) 43301.
[50] Q. Xiong, A.Y. Nikiforov, X.P. Lu, C. Leys, High-speed dispersed photographing of an open-air argon plasma plume by a grating-ICCD camera system, J. Phys. D: Appl. Phys. 43 (2010) 415201.
[51] X. Lu, Z. Jiang, Q. Xiong, Z. Tang, Y. Pan, A single electrode room-temperature plasma jet device for biomedical applications, Appl. Phys. Lett. 92 (2008) 151504.
[52] X. Lu, Z. Jiang, Q. Xiong, Z. Tang, X. Hu, Y. Pan, An 11 cm long atmospheric pressure cold plasma plume for applications of plasma medicine, Appl. Phys. Lett. 92 (2008) 81502.
[53] J. Jansky, F. Tholin, Z. Bonaventura, A. Bourdon, Simulation of the discharge propagation in a capillary tube in air at atmospheric pressure, J. Phys. D: Appl. Phys. 43 (2010) 395201.
[54] D. Breden, K. Miki, L.L. Raja, Self-consistent two-dimensional modeling of cold atmospheric-pressure plasma jets/bullets, Plasma Sour. Sci. Technol. 21 (34011) (2012).
[55] I. Jogi, R. Talviste, J. Raud, K. Piip, P. Paris, The influence of the tube diameter on the properties of an atmospheric pressure He micro-plasma jet, J. Phys. D: Appl. Phys. 47 (2014) 415202.
[56] H. Cheng, X. Lu, D. Liu, The effect of tube diameter on an atmospheric-Pressure micro-Plasma jet, Plasma Process Polym. 12 (2015) 1343–1347.
[57] J. Hubert, T. Dufour, N. Vandencasteele, S. Desbief, R. Lazzaroni, F. Reniers, Etching processes of polytetrafluoroethylene surfaces exposed to he and He-O-2 atmospheric post-discharges, Langmuir 28 (2012) 9466–9474.
[58] N. Vandencasteele, B. Broze, S. Collette, C. De Vos, P. Viville, R. Lazzaroni, F. Reniers, Evidence of the synergetic role of charged species and atomic oxygen in the molecular etching of PTFE surfaces for hydrophobic surface synthesis, Langmuir 26 (2010) 16503–16509.
[59] E.A.D. Carbone, N. Boucher, M. Sferrazza, F. Reniers, How to increase the hydrophobicity of PTFE surfaces using an r.f. atmospheric-pressure plasma torch, Surf. Interface Anal. 42 (2010) 1014–1018.
[60] T. Dufour, J. Hubert, P. Viville, C.Y. Duluard, S. Desbief, R. Lazzaroni, F. Reniers, PTFE surface etching in the post-discharge of a scanning RF plasma torch: evidence of ejected fluorinated species, Plasma Process Polym. 9 (2012) 820–829.
[61] Z. Fang, Y. Qiu, Y. Luo, Surface modification of polytetrafluoroethylene film using the atmospheric pressure glow discharge in air, J. Phys. D: Appl. Phys. 36 (2003) 2980–2985.
[62] F. Fanelli, F. Fracassi, R. D'Agostino, Fluorination of polymers by means of He/CF4-fed atmospheric pressure glow dielectric barrier discharges, Plasma Process Polym. 5 (2008) 424–432.
[63] M. Morra, E. Occhiello, R. Marola, F. Garbassi, P. Humphrey, D. Johnson, On the aging of oxygen plasma-treated polydimethylsiloxane surfaces, J. Colloid Interface Sci. 137 (1990) 11–24.
[64] C.C. Dupont-Gillain, Y. Adriaensen, S. Derclaye, P.G. Rouxhet, Plasma-oxidized polystyrene: wetting properties and surface reconstruction, Langmuir 16 (2000) 8194–8200.
[65] L. Nguyen, M. Hang, W. Wang, Y. Tian, L. Wang, T.J. McCarthy, W. Chen, Simple and improved approaches to long-Lasting hydrophilic silicones derived from commercially available precursors, Acs Appl. Mater. Int. 6 (2014) 22876–22883.
[66] F. Chen, J. Liu, Y. Cui, S. Huang, J. Song, J. Sun, W. Xu, X. Liu, Stability of plasma treated superhydrophobic surfaces under different ambient conditions, J. Colloid Interface Sci. 470 (2016) 221–228.
[67] R.C. Chatelier, X. Xie, T.R. Gengenbach, H.J. Griesser, Quantitative analysis of polymer surface restructuring, Langmuir 11 (1995) 2576–2584.
[68] E. Robert, M. Vandamme, L. Brullé, S. Lerondel, A. Le Pape, V. Sarron, D. Riès, T. Darny, S. Dozias, G. Collet, C. Kieda, J.M. Pouvesle, Perspectives of endoscopic plasma applications, Clin.l Plasma Med. 1 (2013) 8–16.